Vol. 40, No. 1 (2018), 117-128, DOI: 10.24874/ti.2018.40.01.11

Tribology in Industry

www.tribology.rs

RESEARCH

Thermal and Dry Sliding Wear Behavior of Plasma Sprayed Red Mud-Fly Ash Coatings on Mild Steel

H. Sutar[a, b, c], D. Roy[a], S.C. Mishra[b], S. Patra[c], R. Murmu[c]

[a] *Chemical Engineering Department, Jadavpur University, Kolkata, Pin-700032, India,*
[b] *Metallurgical and Materials Engineering Department, National Institute of Technology, Rourkela, pin-769008, India,*
[c] *Chemical Engineering Department, Indira Gandhi Institute of Technology, Sarang, pin-759146, India.*

Keywords:

Red mud
Fly ash
Morphology
Bond strength
Thermal stability
Sliding wear

Corresponding author:

Harekrushna Sutar
Jadavpur University, Kolkata,
West Bengal, Pin-700032, India.
E-mail: h.k.sutar@gmail.com

A B S T R A C T

The present work focuses to understand the limitations towards high temperature applications of plasma sprayed coatings like pure red mud, composited with varying weight % (10, 20 and 50) of fly ash on mild steel. Spraying is done at different operating power namely 9, 12 and 15 kW. Coating characteristics like morphology, thickness and phase formations are studied. The sustainability of these coatings towards high temperature at air environment up to 1000 °C is evaluated by finding their adhesion strength. DSC and TGA techniques are implemented to observe the coating behavior to heat. The coatings show remarkable resistance towards high temperature by virtue of adhesion strength compensation. It is feasible to use these coatings <800 °C, otherwise dislodging of coating from metal. Finally sliding wear performances are seen using a pin on disc tribometer at track diameter of 100 mm, sliding speed of 100 rpm (0.523 m/s) and normal load of 10 N with 3 minute incremental time interval up to 51 minute. Sliding time is seen to be remarkable variable for wear rate. Reinforcement of fly ash leads to form stronger bond strength with mild steel. Wear experiments are designed by Taguchi optimization technique to conclude the optimum variable impacting it.

1. INTRODUCTION.

The disposal of red mud (RM) in the present scenario is alarming the environment globally. Alternative routes for its potential reuses are a matter of concern. We have reported broadly a review [1]. Red mud has been used as a reinforcing material in different metals to enhance their mechanical properties [2,3]. But, coating technology may be an alternative for its suitability. The present work is an attempt to develop wear resistive coatings towards better tribological applications. Some conventional wear resistive coating materials are nickel, iron, cobalt and molybdenum based alloys, carbides of ceramic and tungsten. Coating developed by Plasma spraying technology is found to be more acceptable due to its amplified surface characteristics. Literature reviews [4] the surface behavior of pure red mud coatings. Still

research progress on red mud coatings is limited. We developed a coating by reinforcing 10, 20 and 50 % fly ash (FA) by weight to red mud by atmospheric plasma spray technology (APS). No relevant work is found on its high temperature application areas.

Interfaces that are usually exposed to elevated temperatures are of various moving assemblies in the aerospace industry, power generation and metal working processes [5]. Metallic or metallic alloy coatings when exposed to above 200 °C; most of them lose their initial properties and soften appreciably [6]. So such coatings are limited to low temperature applications. To offset, it is needful to design a coating that can pass the high temperature climate. History reveals Ni-Cr alloy as a widely used coating material on mild steel. But the outlook of Ni-Cr alloy is dark due to its increasing demand. To replace Ni-Cr alloys, a project was undertaken by United States National Bureau of Standards by ceramic coated steel in number of applications [7]. The Bureau considered several factors specially importance for coatings suitability to high temperature such as high bond strength, low thickness, no re-boil, protection of steel against oxidation and high resistance to thermal shock.

Development of ceramic coatings is resuming a promising momentum towards high temperature applications areas, owing to its greater refractoriness and bond strength. The adhesive (bond) strength of coating sprayed onto a metal substrate is usually considered due to mechanical anchoring, chemical (metallurgical) bonding, and van der Waals forces [8]. The roughness of the substrate is a major influencing factor on adhesive strength [9]. The roughened surface enhances mechanical anchoring of the coating, and the clean surface can also be expected to strengthen metallurgical bonding and physical bonding between the coating and the substrate [10]. Literature reveals bond strength of Al–Si coating on mild steel by kinetic spraying deposition technique [11]. Results of adhesion measurements for different systems of steel sheet-phosphate inter layer ceramic coating are described [12,13].The development of new coating technological methods is still in progress. Relatively simple and low-cost manufacturing technique of thermal barrier coatings has been developed, which is called the slurry spray technique [14]. A broad description of physics of different coatings and their application are reported [15]. Fly ash/quartz/illmenite composite coatings developed by means of plasma spraying technique on copper metal are revealed [16].

Coating feasibility is also computed from its wear resistive properties. The tribological behavior of coatings is affected by several factors; namely geometry of contact, material characteristics, basic mechanical properties, operating parameters controlling the coating deposition and finally the microstructure [17]. Ceramic coatings show better tribological applications [18], but failure mechanisms like plastic deformations, brittle fracture and polish effect difficulties are reported [19]. Hence demand for reinforcing these coatings with additives for improving wear behavior increases.

The scope of the research to evaluate the limitations of plasma sprayed red mud and its composite coatings with fly ash. We have augmented 10, 20 and 50 % fly ash by weight to red mud. Adhesion strength at elevated temperatures is discovered. Effect of operating power on surface morphology, chemical bonding, thickness and wear are checked. Taguchi optimization technique is implemented to ascertain the controlling variable to wear.

2. EXPERIMENTAL

2.1 Collection of raw material

The chief raw material used in the experiment is red mud, collected in powder form, from NALCO, Damojodi, India. Fly ash is availed from captive power plant of Rourkela Steel Plant, India. As received powder materials are dried under sunlight to make it bone dry, grinded in ball mill and sieved to obtain 90-110 μm size range particles. In order to recognize the constituents of red mud and fly ash, the SEM (JEOL; JSM 6480 LV) and EDS analysis are performed and reported in Fig. 1.

Fly ash powder is mixed manually with red mud powder to obtain the composite. Different weight % of fly ash namely 10, 20 and 50 % by weight are prepared separately

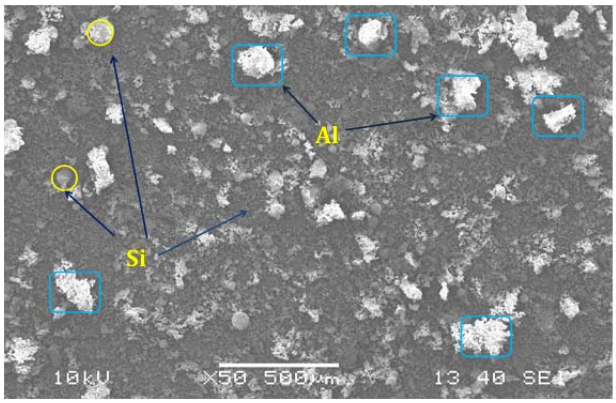

(a)

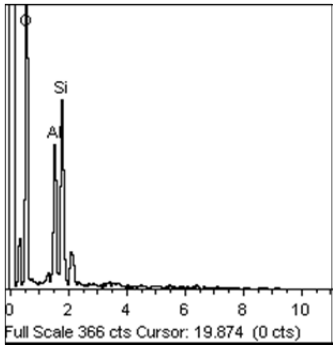

(b)

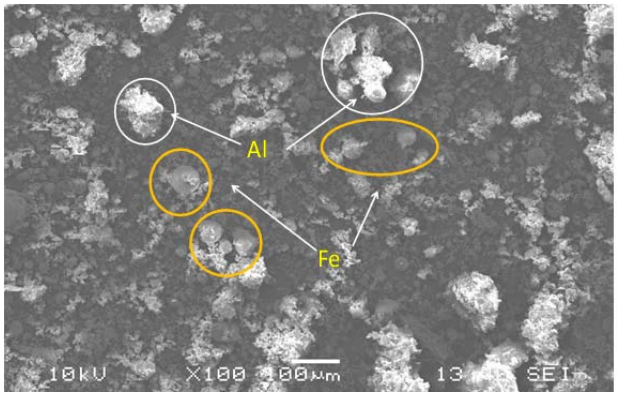

(c)

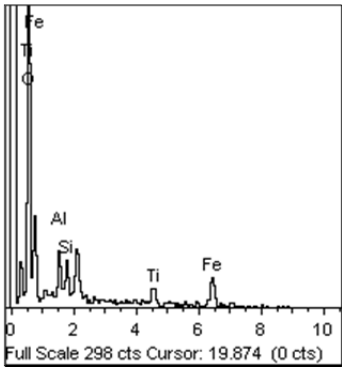

(d)

Fig. 1. SEM and EDS analysis reports for (a), (b) Fly Ash and (c), (d) Red Mud.

Composite powders are blended using an in house rotating V-shaped blender to obtain a homogeneous powder. Directly after the present time, the powder material goes for plasma spraying unit for coating.

2.2 Arrangement of Substrate

Mild steel is incorporated for the present work as base material for coating. Three different shaped objects are fabricated on which coating is developed. For wear analysis mild steel rod is cut up to cylindrical shape, l =40 mm and Φ= 15 mm. Spraying is done on one side cross section. In order to measure the adhesion strength, substrates of rectangular shape (100 × 90 × 10 mm) are produced and coated with, no part left out. For the convenience of DSC and TGA experiments, substrates of circular shape, Φ= 5 mm and thickness 2 mm are designed and fully coated. Prior to coating, specimens are passed through grit blasting at a pressure of 5 kg/cm^2 aiding alumina grits of size 80 to obtain mean surface roughness of 5.7 μm. Following, sample pieces are cleaned in an ultrasonic cleaning unit and proceeds for immediate coating.

2.3 Plasma Spraying

Typical atmospheric plasma spraying (APS) technique is adopted to coat the available raw material. The APS is availed from Hindustan Aeronautics Limited (HAL), Sunabeda, India. Operating power is regulated by varying the input current and voltage to the plasma gun. The powder raw material is fed at 20 gm/min, using a turntable type volumetric powder feeder. Input power to the plasma gun is retained at namely 9, 12 and 15 kW. Spraying is conducted at 90° to achieve maximum coating deposition efficiency. Argon, Nitrogen gases are used as primary and secondary plasma generating medium.

2.4 Pin on disc wear test configuration

A laboratory tribometer (MAGNUM Engineers, Bangalore, India) is put into effect to find wear rate (mass loss in gm) as per ASTM G-99 standard. The tool primarily consists of a stationary pin under an applied load in contact with a rotating hardened ground steel disc (En-32, 65 HRC, R_a= 0.5 μm), combination of computer control and tribox software, a pulley and lever arrangement as visible in Fig. 2. The unit can measure wear properties both in lubricated and dry sliding conditions. The disc is driven by a 2.5 HP motor capable of running at 0–1500 rpm. All wear tests are conducted at a

fixed track diameter, 100 mm, sliding speed, 100 rpm and at applied normal load of 10 N. Wear performances are managed at ambient conditions and results are repeatable.

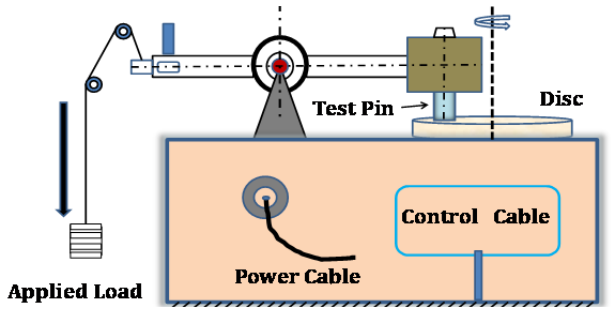

Fig. 2. Outline of prevailing pin on disc tribometer.

2.5 Taguchi Optimization

Design of Experiments (DOE) is one of the important and powerful statistical techniques to study the influence the various controlling factors on performance output. All designed experiments require a certain number of combinations of factors and levels be tested in order to observe the results of those test combination. Taguchi optimization procedure is employed to find the optimum operating parameters influencing the wear using MINITAB-16. Dry sliding tests are carried out up to 51 minutes. To understand the effect of time, we have considered 15, 30 and 45 minute intervals to fit the design performance. The operating conditions implemented are given in Table 1.

Table 1. Levels of the variables used in the experiment.

Control Factors	Level			
	I	II	III	Unit
A: Time	15	30	45	Minute
B: Power	9	12	15	kW
C: FA Content	10	20	50	wt%

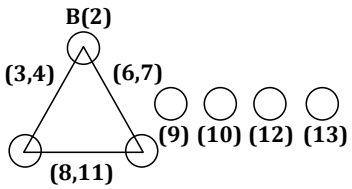

Fig. 3. Standard linear graphs for L_{27} array.

Design is conducted in accordance with L_{27} (3^{13}) orthogonal array and corresponding linear graph is shown in Fig. 3. The S/N ratios for minimum wear rate "in gm" under 'smaller is the better characteristic', can be calculated as the logarithmic transformation of the loss function as shown below.

Smaller is the better characteristic:

$$\frac{S}{N} = -10 \log \frac{1}{n} (\sum y^2) \quad (1)$$

Where 'n' is the repeated number trial conditions and 'y' is the sliding wear data.

3. RESULTS AND DISCUSSION

3.1 Morphology, hardness, composition and thickness before bond test

Coating surface characteristics are controlled by inter particle bonding of powder materials during plasma melting. Adhesion strength of the coating layers to the metal substrate dominates the surface behaviour.

The existing research focuses, how the plasma torch input power decides the coating floors. Is there any changes arise to coating layers, after fly ash augmentation? Electron microscopy images are exercised to reveal it. Figure 4 reports the surface modifications for; (a) red mud, (b) red mud + 10 % FA, (c) red mud + 20 % FA and (d) red mud + 50 % FA at magnification × 30 for 12 kW input. Particles are broadly distributed for pure red mud and seem to be even throughout.

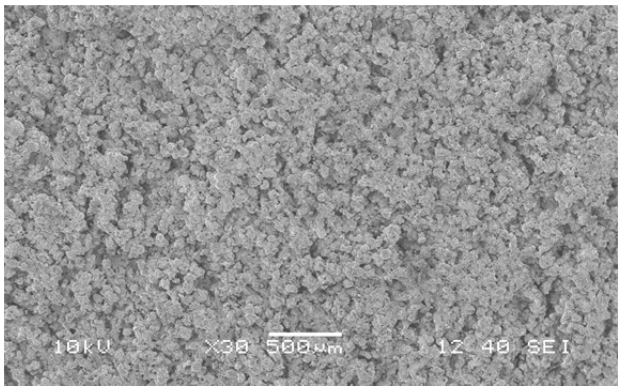

(a)

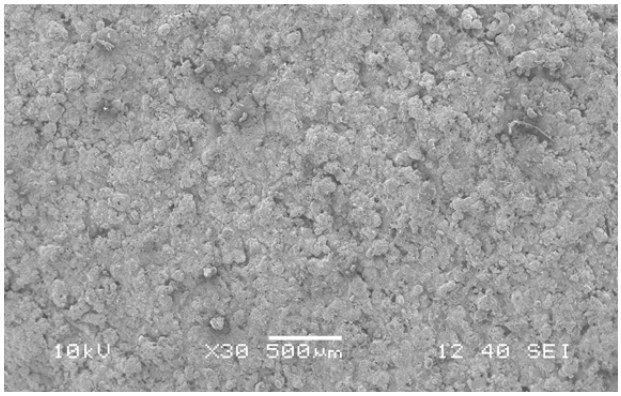

(b)

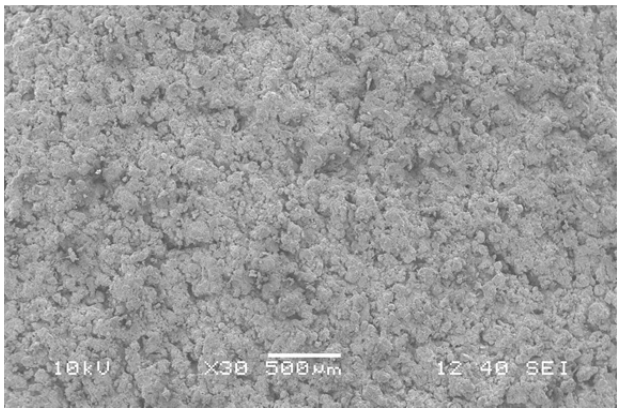

(c)

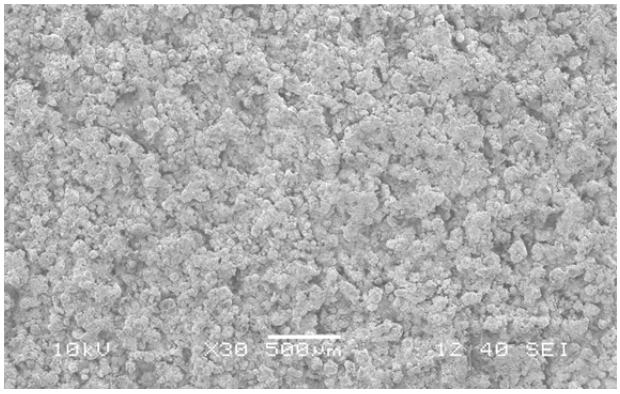

(d)

Fig. 4. Surface responses for; (a) RM, (b) RM + 10 % FA, (c) RM + 20 % FA and (d) RM + 50 % FA Coatings at 12 kW operating power at ×30.

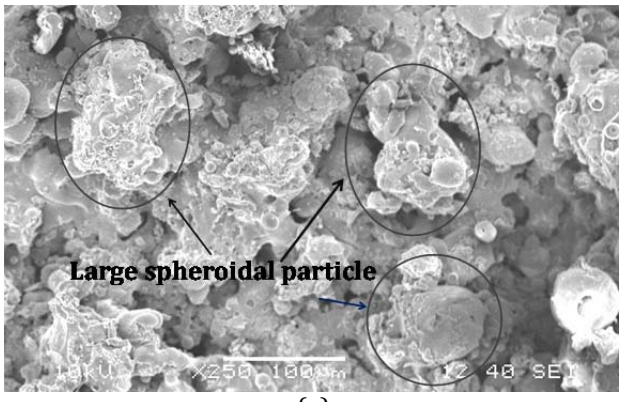

(a)

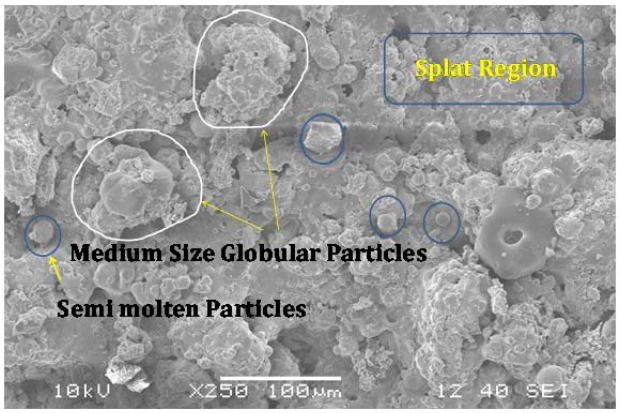

(b)

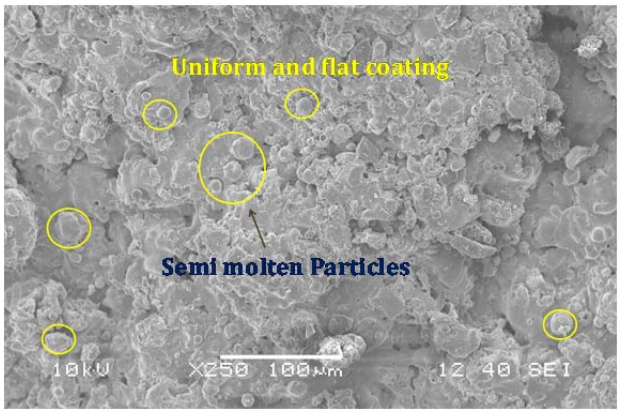

(c)

Fig. 5. Morphology of RM + 20 % FA coatings made at (a) 9 kW, (b) 12 kW and (c) 15 kW of plasma torch input power at ×250.

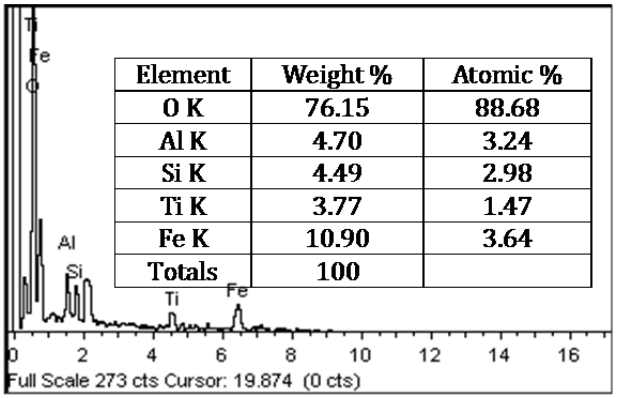

Element	Weight %	Atomic %
O K	76.15	88.68
Al K	4.70	3.24
Si K	4.49	2.98
Ti K	3.77	1.47
Fe K	10.90	3.64
Totals	100	

(a)

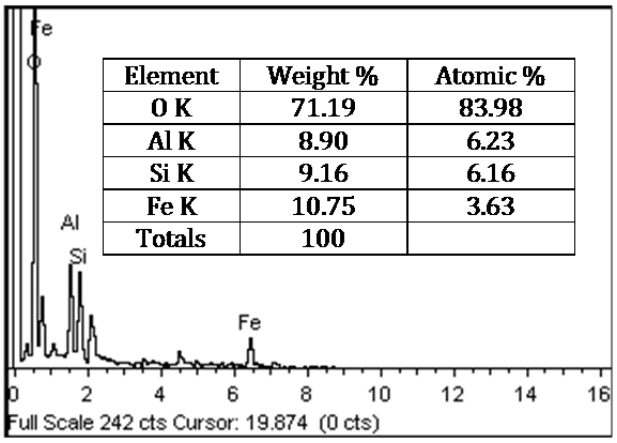

Element	Weight %	Atomic %
O K	71.19	83.98
Al K	8.90	6.23
Si K	9.16	6.16
Fe K	10.75	3.63
Totals	100	

(b)

Fig. 6. EDS records, (a) RM + 10 % FA and (b) RM + 50 % FA coatings at 12 kW operating power.

The reinforcement of fly ash to red mud results in more agglomeration of particles leading to a lumpy, non-uniform and a coarser exterior. The coating morphology is extensively affected by plasma torch input power. Figure 5 reveals the outcomes at magnification ×250. It is believed that the plasma flame temperature increases with input power, dominating the mechanism of

coating. Rise of flame temperature, plays a significant role on surface chemistry of prevailing coatings. At 9 kW, large spherical particles are seen, might be due to improper melting of coating precursor. Surface seems to be rougher with spotted cavities. As the input power increases, the surface topology modifies to a flatter, homogeneous film with less spotted cavities and pores.

Harness of the prevailing coatings plays an important role to characterize the wear rate. Data pertaining to hardness of our coatings are reported can be obtained from reference [20]. Compositions of the coatings are acknowledged by means of EDS and XRD (Philips X-Ray diffractometer) analysis. Coating elements are reviewed and recorded in Fig. 6 for 12 kW power supply. Figure 6(a) illustrates the elements available in RM + 10 % FA coating. Augmentation of FA to RM makes the coating more Si and Al enriched, corresponding to Fig. 6 (b). Further compositions of coatings are investigated with respect to operating power.

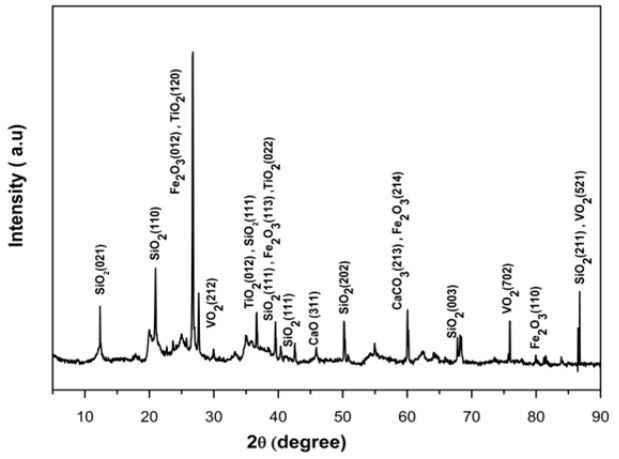

(a)

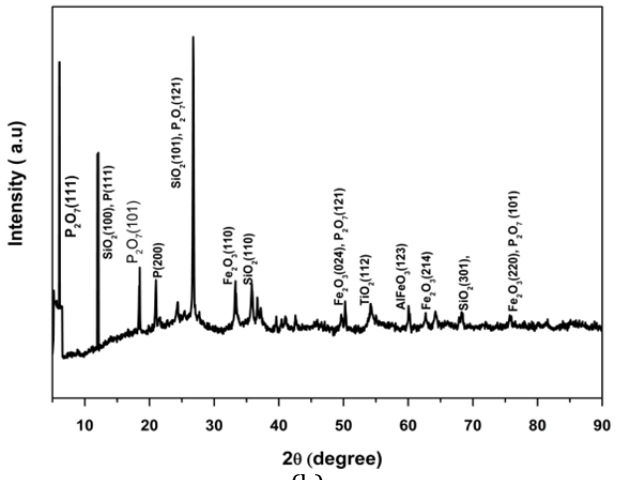

(b)

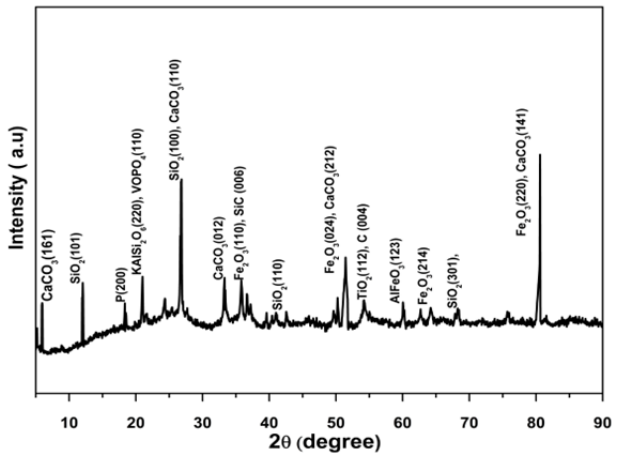

(c)

Fig. 7. X-Ray diffractogram of RM + 50 % FA Coatings at (a) 9 kW, (b) 12 kW and (c) 15 kW operating power levels.

XRD techniques are executed to realize it and reported in Fig. 7 for RM + 50 % FA coatings. The major phases are iron oxide (Fe_2O_3), Silicon dioxide (SiO_2) and minor phase like Titanium dioxides (TiO_2) are visible for 9 kW power level. But as the spraying power alters to 12 kW, the anatomy of coatings is rephrased. The major phases are reconstructed to Pyrophosphate (P_2O_7).At the other end, for 15 kW, numbers of shortened peaks are observed. Majority of peaks confirms Calcite ($CaCO_3$) compound.

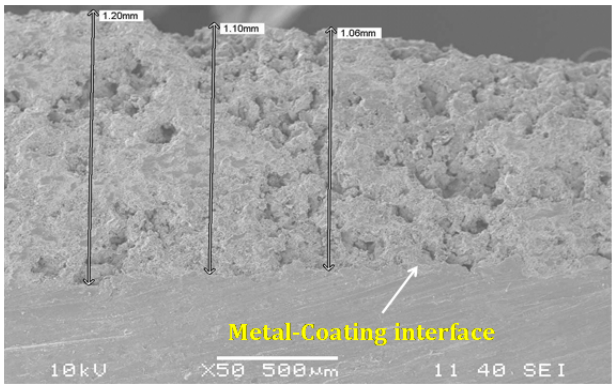

(a)

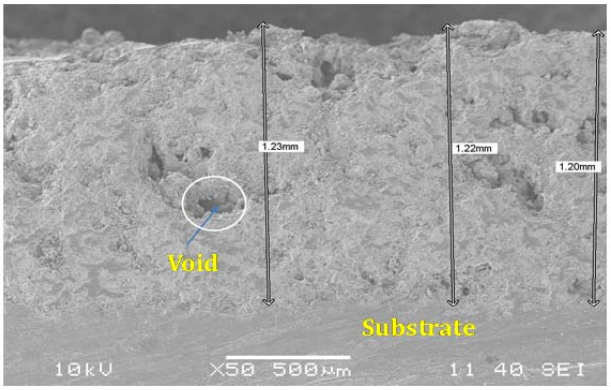

(b)

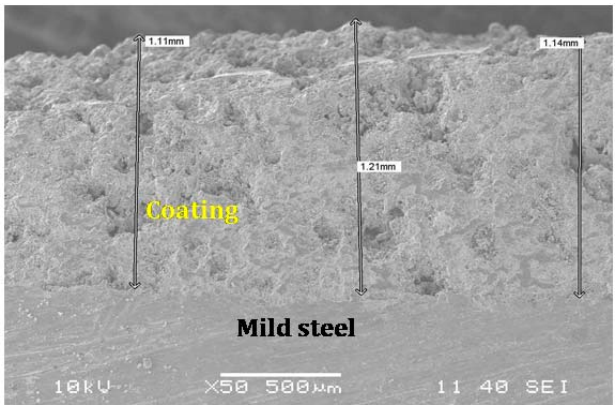

(c)

Fig. 8. Section Microstructure of RM + 20 % FA Coatings at (a) 9 kW, (b) 12 kW and (c) 15 kW.

Figure 8 shows cross sections of mild steel coated with RM + 20 % FA with different operating power. At 9 kW, most of the coated inter sections are porous. Air voids has occupied from metal-coating interface to the tip. Increase of plasma operating power (alternatively plasma temperature) promotes a better metallurgical union and agglomeration between the melted particles. So at higher temperature, it is believed that, molten particles get adhered to the substrate at sufficient strength. Minimum air voids are noticed with a smooth structure. Observation on thickness indicates a marginal change with power.

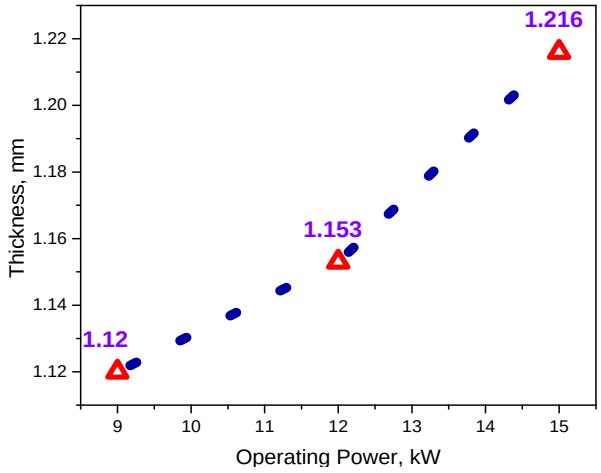

Fig. 9. Action of operating power on thickness.

Figure 9 manifests that, improvement of the coating thickness is relatively narrow with operating power. The average thickness for 9 kW is 1.12 mm and rises up to 1.216 mm for 15 kW. The rise in power possibly enhances the thermal flux, leading to, enthalpy gain by the molten particles, resulting in improved deposition volume.

3.2 TGA, DSC and bond strength analysis at elevated temperatures

The first two thermal analysis techniques used were thermogravimetric analysis (TGA) as per ASTM E-2008 standards and differential scanning calorimeter (DSC) applying Setaram DSC 131 analyser. The temperature parameters for the DSC experiments are fixed from room temperature to 1000 °C at a heating rate of 10 °C/min in oxidative environment, with air flow rate 10 ml/min. Analysis in this section is focused for coatings made at 12 kW only. Originated TGA curve for the prevailing coatings are shown in figure-10. Weight loss is maximum (up to 89.6 %) for RM + 50 % FA coatings whereas minimum (up to 95 %) for pure red mud coatings. Up to about 250 °C, no significant weight loss is seen. Here after, the loss is abrupt and becomes stagnant at around 600 °C. Reinforcement of FA to RM results in enrichment in Si and Al content (Fig. 6b), building a more hygroscopic composite. The Si enriched coatings, tends to carry supplementary moisture and dehydrates in great. Behaviour of the coatings to heat exposure is revealed in Fig. 11. Heat carrying capacity is higher for FA composited coatings. Pure RM coatings absorb heat up to a critical temperature of approximately 650 °C and then start to release. Whereas the FA (10 %) based coatings continue to gain heat till 750 °C. Results are presuming to higher Al content of the FA composited coatings, leading a film of intensified thermal conductivity. But the cause of alternation of heating behaviour at critical point is not recognizable.

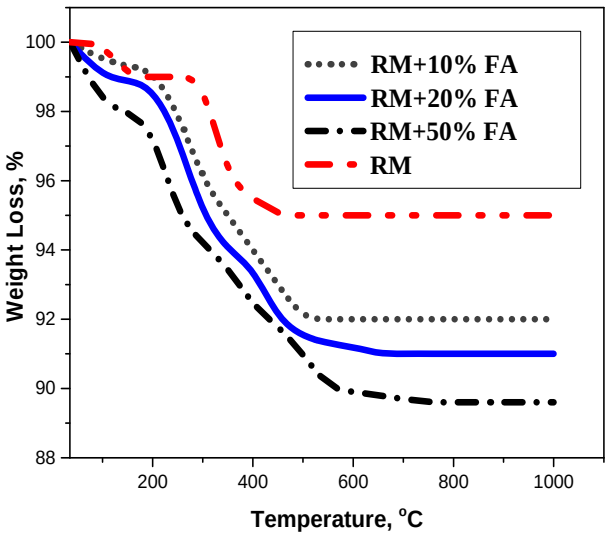

Fig. 10. TG analysis of coatings.

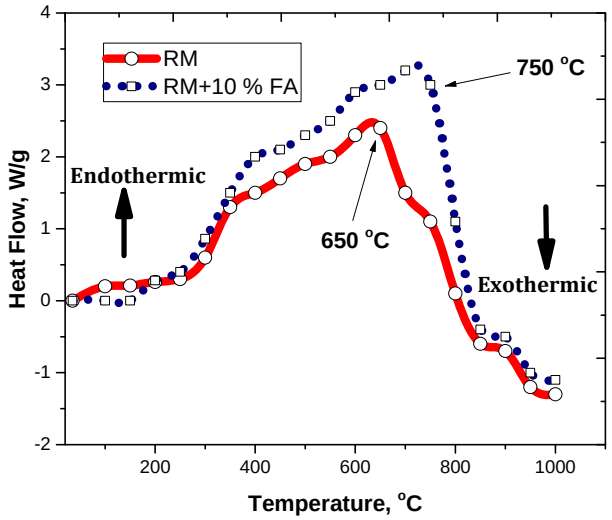

Fig. 11. Originated DSC plot of coatings.

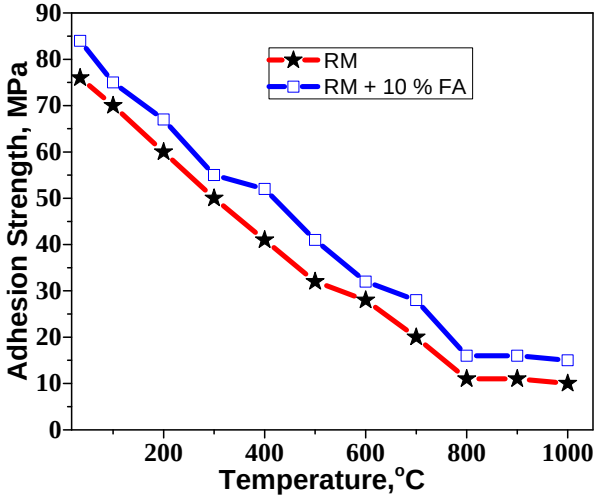

Fig. 12. Influence of temperature on bond strength.

Finally we have measured adhesion strength of coatings at an interval of 100 °C up to 1000 °C. Coated specimens are heat treated using a muffle furnace at each desired temperature for 2 hour. Specimens are then allowed to cool under normal atmosphere to reach air temperature and adhesion strength is measured, using a Caltech BGD 1520 digital pull off adhesion tester with 10 mm dolly as per ASTM D4541 standards. Both resin and hardener mixed in equal proportion and used as adhesive. Bond strengths are reported corresponding to adhesive failure of coatings. Figure 12 reveals the strength results of coatings. Bond strength falls with temperature. Reinforcement of FA boosts the adhesive strength, might be due to enhancement of interfacial affinity of fly ash molecules to mild steel during melting and origination of coating. Bond strength declines linearly with rise in temperature and stabilises at approximately 800 °C.

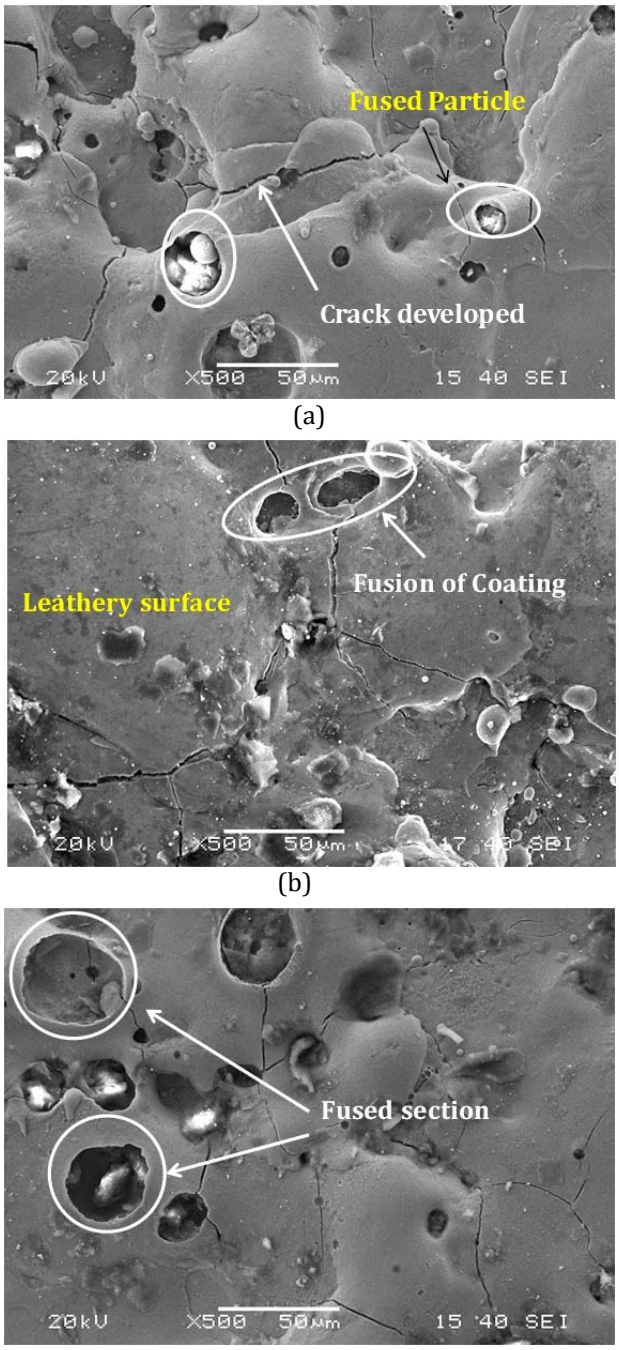

Fig. 13. Cracked surfaces of RM + 10 % FA coatings at (a) 800 °C, (b) 900 °C and (c) 1000 °C.

Microstructural stability is a critical factor influencing the thermal and mechanical behaviour of ceramic coatings. Modifications of coating surfaces are seen after 800 °C. Few microscopic images are captured in Fig. 13 to recognize the surface morphology at high temperatures. It is observed that, at elevated temperature (>800 °C) the coatings "soften" causing sheets to stick and fuse. However, the most common associated problem is "cracking".

Table. 2. Experimental design using L_{27} orthogonal array.

L_{27} (3^{13})	Time (Min)	Power (kW)	FA Content %	Wear rate (gm)	S/N Ratio (dB)
1	15	9	10	0.0150794	36.4323
2	15	9	20	0.0125000	38.0618
3	15	9	50	0.0088000	41.1103
4	15	12	10	0.0130000	37.7211
5	15	12	20	0.0100000	40.0000
6	15	12	50	0.0040000	47.9588
7	15	15	10	0.0141000	37.0156
8	15	15	20	0.0110000	39.1721
9	15	15	50	0.0060000	44.4370
10	30	9	10	0.0329865	29.6333
11	30	9	20	0.0250000	32.0412
12	30	9	50	0.0242000	32.3237
13	30	12	10	0.0281000	31.0259
14	30	12	20	0.0222000	33.0729
15	30	12	50	0.0200000	33.9794
16	30	15	10	0.0300000	30.4576
17	30	15	20	0.0248000	32.1110
18	30	15	50	0.0230000	32.7654
19	45	9	10	0.0365480	28.7427
20	45	9	20	0.0320000	29.8970
21	45	9	50	0.0317000	29.9788
22	45	12	10	0.0326000	29.7356
23	45	12	20	0.0282000	30.9950
24	45	12	50	0.0267000	31.4698
25	45	15	10	0.0360000	28.8739
26	45	15	20	0.0299000	30.4866
27	45	15	50	0.0281000	31.0259

Web-like pattern of fine cracks develop on coating, causing it to resemble cracked and a leathery skin. Enrichment of Si leads to the formation of brittle phases which may reduce the scale adherence due to continuous heat exposure. Probably Si reacts with the other species, forming damaging compounds and destroys the bonding between the mild steel and the coating.

3.3 Sliding wear design

The sliding wear behaviour is designed and published in Table 2. The mean of the S/N ratios is found to be 35.30 dB. Figure 14 shows graphically the effects of controlling factors on wear rate. Smaller the better characteristic was taken for this analysis. The responses for signal to noise ratios to wear rates are reported in Table 3. It is concluded that, time is the most dominating factor to wear, followed by composition and power.

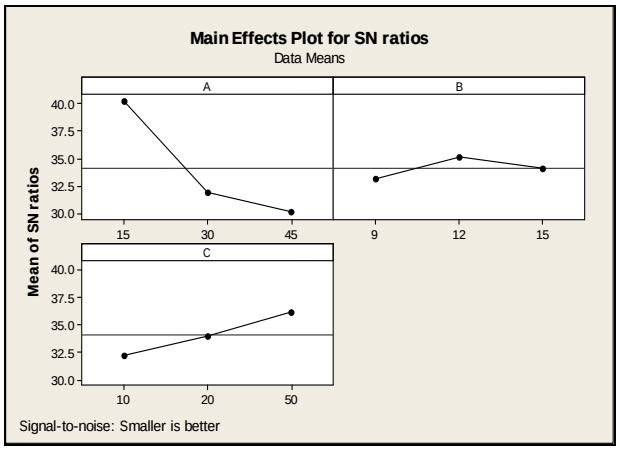

Fig. 14. Effect of control factors on wear rate.

Result analysis from Fig. 14 concludes that a factor combination of A_1, B_2 and C_3 shows a minimum wear rate. The interaction plots are shown in Fig. 15. The analysis of variance (ANOVA) was used to analyze the influence of wear parameter.

Table 3. Response table to wear.

LEVEL	A	B	C
1	40.21	33.14	32.18
2	31.93	35.11	33.98
3	30.13	34.04	36.12
Delta	10.08	1.97	3.93
Rank	1	3	2

The ANOVA establishes the relative significances of factors in terms of their percentage contribution to the response. This analysis was carried out for a level of significance of 5 % (the level of confidence 95%). 'P' value, less than 0.05 for a particular parameter, indicates that it has the major effect on the responses. Last column in Table 4 shows the effect of individual parameters on the responses. Observations from Fig. 15 and Table 4 conclude that the interaction between A×B shows minimum effect on wear. The combination of factors A and C has the major effect on wear. The factor B has least contribution on wear rate. But its combination with factor 'C' has significant effect on wear rate. The correlation between coating removal rate, CRR (non-variable factor) and variable factors (time, power and FA content) was found by multiple linear regressions from the equation 2.

$$CRR = K_0 + K_1A + K_2B + K_3C. \quad (2)$$

where, K_i (i= 0, 1, 2, 3....) is a model constant. The regression equation is:

$$CRR\ (gm) = 0.00947 + 0.000694\ A - 0.000295\ B - 0.000161\ C. \quad (3)$$

From equation 3 it is observed that time has a major impact on wear, followed by composition and operating power. Confirmation experiment is the final test in the design of the experiment process. The purpose of confirmation experiment is to validate the conclusions drawn during the analysis phase. From the model, result of confirmation test is reported in Table 5.

Table 4. ANOVA table for wear rate.

Source	DF	Seq SS	ADj SS	Adj MS	F	P	% P	Rank
A	2	0.0020801	0.0020801	0.0010400	1747.64	0.000	86.06	1
B	2	0.0000644	0.0000644	0.0000322	54.08	0.000	2.66	3
C	2	0.0002486	0.0002486	0.0001243	208.84	0.000	10.27	2
A×B	4	0.0000016	0.0000016	0.0000004	0.65	0.642	0.07	3
B×C	4	0.0000024	0.0000024	0.0000006	0.99	0.465	0.09	2
A×C	4	0.0000162	0.0000162	0.0000041	6.81	0.011	0.66	1
Error	8	0.0000048	0.0000048	0.0000006			0.19	
Total	26	0.002417						

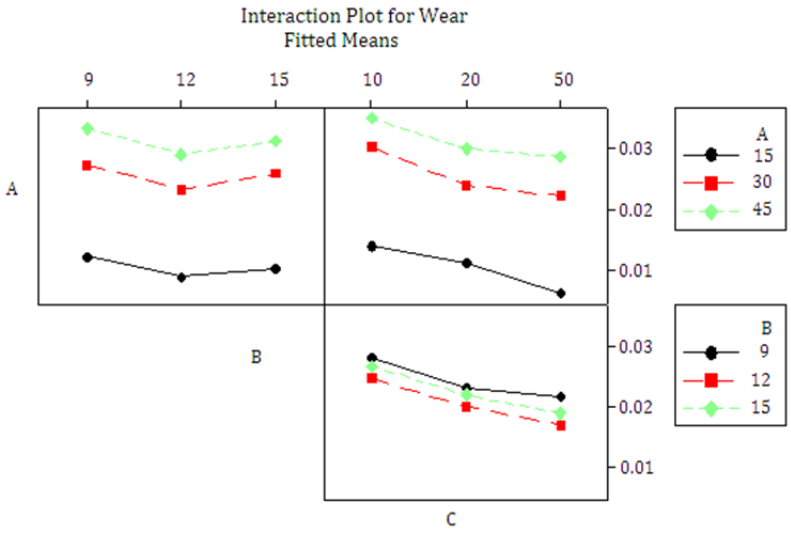

Fig.15. Interaction graph between A×B×C for wear rate.

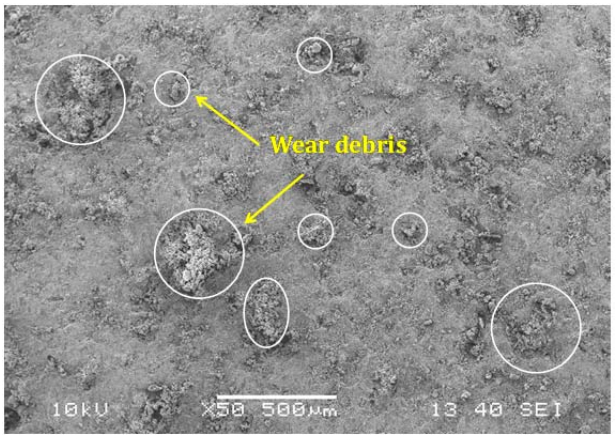

(a)

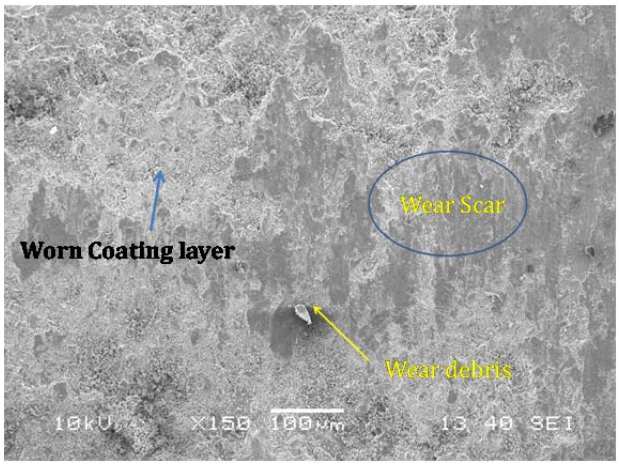

(b)

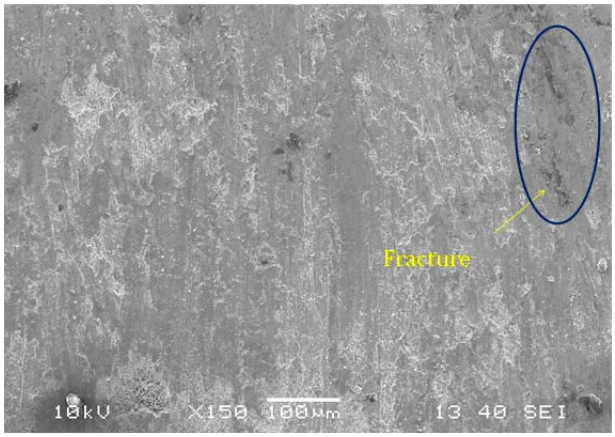

(c)

Fig. 16. Wear morphology of red mud coating made at 9 kW after (a) 15, (b) 30 (c) 45 minute of sliding.

Table 5. Results of the confirmation experiments.

	Optimal control parameters	
	Prediction	**Experimental**
Level	$A_1B_2C_3$	$A_1B_2C_3$
S/N ratio of wear rate, dB	46.8563	47.9588

An error of 2.35 % for the S/N ratio of wear rate is observed. Wear morphology for pure red mud coatings made at 9 kW are pictured in Fig. 16. It is visible that, wear surface behaviour modifies with time, leading to alternation of contact mechanism. It is believed that, wear takes place primarily by abrasion mechanism, pertaining to the shear stress between the two surfaces in contact. With time, most of the wear debris disappear and fracture development initiates.

4. CONCLUSION

The present experimental study concludes that, red mud coatings possess high thermal resistance properties. Fly ash is a beneficiary reinforcing agent for red mud, and the composite can be coat able with favouring surface properties. Coatings can be operated at high temperature. It is observed that, these composite coatings can also be employed for suitable tribological applications. Plasma generating power, adversely affect the coating morphology. Taguchi optimization remarks, time is the most dominating to wear. Although operating power is least affected to wear; but it cannot be neglected, due to significant interaction with other parameters. Our work is a portfolio for researcher to discover many other aspects of red mud and its composite coatings. Study of corrosion wear behaviour may be implemented by future investigators to find its distinct application areas.

REFERENCES

[1] H. Sutar, S.C. Mishra, S.K. Sahoo, A.P. Chakraverty, H.S Maharana, *Progress of red mud utilization: An overview*, American Chemical Science Journal, vol. 4, iss. 3, pp. 255-279, 2014, doi: 10.9734/ACSJ/2014/7258

[2] N. Panwar, R.P. Poonia, G. Singh, R. Dabral, A. Chauhan, *Effect of Lubrication on Sliding Wear of Red Mud Particulate Reinforced Aluminium Alloy 6061*, Tribology in Industry, vol. 39, no. 3, pp. 307-318, 2017, doi: 10.24874/ti.2017.39.03.05

[3] R. Dabral, N. Panwar, R. Dang, R.P. Poonia, *A. Chauhan, Wear Response of Aluminium 6061 Composite Reinforced with Red Mud at Elevated Temperature*, Tribology in Industry, vol. 39, no. 3, pp. 391-399, 2017, doi: 10.24874/ti.2017.39.03.14

[4] A. Satapathy, H. Sutar, S.C. Mishra, S.K. Sahoo, *Characterization of plasma sprayed pure red mud*

coatings: An analysis, American Chemical Science Journal, vol. 3, iss. 2, pp. 151-163, 2013, doi: 10.9734/ACSJ/2013/3218

[5] C. Richard, Tribological *Coatings for high temperature applications*, Encyclopedia of Tribology, New York: Springer, 2011.

[6] M.J.L. Gines, F.J. Williams, C.A. Schuh, *Strategy to Improve the High-Temperature Mechanical Properties of Cr-Alloy Coatings*, Metallurgical and Materials Transactions A, vol. 38, iss. 6, pp. 1367-1370, 2007, doi: 10.1007/s11661-007-9151-4

[7] W.N. Harrison, D.G. Moore, J.C. Richmond, *Ceramic coatings for high-temperature protection of steel*, Part of the Journal of Research of the National Bureau of Standards, vol. 38, pp. 293-307, 1947.

[8] V.V. Sobolev, J.M. Guilemany, J. Nutting, J.R. Miquel, *Development of substrate-coating adhesion in thermal spraying*, International Materials Reviews, vol. 42, iss. 3, pp. 117-136, 1997, doi: 10.1179/imr.1997.42.3.117

[9] S. Adachi, K. Nakata, *Study of Bonding Strength of Plasma-Sprayed Ti-Al Coating on Mild Steel Substrate*, Plasma Processes and Polymers, vol. 4, pp. 512-515, 2007, doi: 10.1002/ppap.200731217

[10] Y.Y. Wang, C.J. Li, A. Ohmori, *Influence of substrate roughness on the bonding mechanisms of high velocity oxy-fuel sprayed coatings*, Thin Solid Films, vol. 485, iss.1-2, pp. 141-147, 2005, doi: 10.1016/j.tsf.2005.03.024

[11] J. Wu, J. Yang, H. Fang, S. Yoon, C. Lee, *Bond Strength of Al-Si Coatings on mild steel by kinetic spraying deposition*, Applied Surface Science, vol. 205, iss. 22, pp. 7809-7814, 2006, doi: 10.1016/j.apsusc.2005.09.015

[12] P. Pokorny, L. Mastny, V. Sykora, Z. Pala, V. Brozek, *Bond Strength of Plasma Sprayed ceramic coatings on phosphate steels*, Metalurgija, vol. 54, no. 2, pp. 411-414, 2015.

[13] S.K. Rahimi, R. Potrekar, N.K. Dutta, N.R. Choudhury, *Anticorrosive interfacial coatings for metallic substrates*, Surface Innovations, vol. 1, iss. 2, pp. 112-137, 2013, doi: 10.1680/si.13.00004

[14] P. Nguyen, S.Y. Ho, A. Kotousov, *Slurry spray technique for manufacturing thermal barrier coatings*, Surface Innovations, vol. 1, iss. 3, pp. 190-199, 2013, doi: 10.1680/si.12.00018

[15] J. Drelich, A. Marmur, *Physics and applications of superhydrophobic and superhydrophilic surfaces and coatings, Surface Innovations*, vol. 2, iss. 4, pp. 211-227, 2014, doi: 10.1680/si.13.00017

[16] A. Behera, S.C. Mishra, *Characteristic study of fly-ash+quartz+illmenite composite coatings on copper substrates*, Emerging Materials Research, vol. 2, iss. 1, pp. 39-44, 2013, doi: 10.1680/emr.12.00025

[17] K. Holmberg, A. Matthews, H. Ronkainen, *Coatings Tribology-Contact Mechanisms and Surface Design*, Tribology International, vol. 31, iss. 1-3, pp. 107-120, 1998, doi: 10.1016/S0301-679X(98)00013-9

[18] L. Somchai, T. Karuna, M. Anchalee, S. Surasak, *Use of MoS_2T coating to reduce wear particles generated in HDD assembly*, Emerging Materials Research, vol. 5, iss. 2, pp. 284-290, 2016, doi: 10.1680/jemmr.16.00089

[19] R. Vijande-Diaz, J. Belzunce, E. Fernandez, A. Rincon, M.C. Perez, *Wear and microstructure in Fine Ceramic Coatings*, Wear, vol. 148, iss. 2, pp. 221-233, 1991, doi: 10.1016/0043-1648(91)90286-4

[20] H. Sutar, D. Roy, S.C. Mishra, A.P. Chakraverty, H.S. Maharana, *Friction and Wear Behaviour of Plasma Sprayed Fly Ash Added Red Mud Coatings*, Physical Science International Journal, vol. 5, iss. 1, pp. 61-73, 2014, doi: 10.9734/PSIJ/2015/12624